

See discussions, stats, and author profiles for this publication at: <https://www.researchgate.net/publication/23771278>

Experimental and theoretical inspection of the phase-to-height relation in Fourier transform profilometry

Article in *Applied Optics* · February 2009
DOI: 10.1364/AO.48.000380 · Source: PubMed

CITATIONS
72


READS
94

4 authors:




Agnès Maurel
École Supérieure de Physique et de Chimie Industrielles
153 PUBLICATIONS **1,333** CITATIONS

SEE PROFILE



Pablo Cobelli
National Scientific and Technical Research Council
28 PUBLICATIONS **416** CITATIONS

SEE PROFILE



Vincent Pagneux
French National Centre for Scientific Research
176 PUBLICATIONS **1,999** CITATIONS

SEE PROFILE



Philippe Petitjeans
École Supérieure de Physique et de Chimie Industrielles
111 PUBLICATIONS **1,281** CITATIONS

SEE PROFILE

Some of the authors of this publication are also working on these related projects:

- Project

PROPASYM : Acoustic asymmetric propagation based on nonlinear processes and time-dependent processes [View project](#)
- Project

Acoustic Metamaterials in the Audible Regime [MetAudible] [View project](#)

Experimental and theoretical inspection of the phase-to-height relation in Fourier transform profilometry

Agnès Maurel,^{1,*} Pablo Cobelli,² Vincent Pagneux,³ and Philippe Petitjeans²

¹Laboratoire Ondes et Acoustique, UMR CNRS 7587, Ecole Supérieure de Physique et Chimie Industrielles, 10 rue Vauquelin, 75005 Paris, France

²Laboratoire de Physique et Mécanique des Milieux Hétérogènes, UMR CNRS 7636, Ecole Supérieure de Physique et Chimie Industrielles, 10 rue Vauquelin, 75005 Paris, France

³Laboratoire d'Acoustique de l'Université du Maine, UMR CNRS 6613, Avenue Olivier Messiaen, 72085 Le Mans Cedex 9, France

*Corresponding author: agnes.maurel@espci.fr

Received 11 September 2008; revised 28 October 2008; accepted 29 October 2008;
posted 18 November 2008 (Doc. ID 100987); published 8 January 2009

The measurement of an object's shape using projected fringe patterns needs a relation between the measured phase and the object's height. Among various methods, the Fourier transform profilometry proposed by Takeda and Mutoh [Appl. Opt. **22**, 3977–3982 (1983)] is widely used in the literature. Rajoub *et al.* have shown that the reference relation given by Takeda is erroneous [J. Opt. A: Pure Appl. Opt. **9**, 66–75 (2007)]. This paper follows from Rajoub's study. Our results for the phase agree with Rajoub's results for both parallel- and crossed-optical-axes geometries and for either collimated or noncollimated projection. Our two main results are: (i) we show experimental evidence of the error in Takeda's formula and (ii) we explain the error in Takeda's derivation and we show that Rajoub's argument concerning Takeda's error is not correct. © 2009 Optical Society of America

OCIS codes: 080.0080, 120.2650.

1. Introduction

The Fourier transform profilometry proposed by Takeda *et al.* in the 80s [1,2] has achieved great success and is now one of the reference techniques for three-dimensional (3D) shape measurement [3–14] (see also a review in [15]). This method uses noncollimated projections of a structured light pattern onto an object (for a review on structured lighting techniques, see [16,17]). The intensity variations of the projected pattern are captured by a camera; afterward, a conversion of the measured phase to the object height is needed. The usually cited phase-to-height relation for noncollimated projection is from Takeda and

Mutoh [2] (both in the parallel- and in the crossed-optical-axes geometries):

$$h(y) = \frac{L\Delta\varphi(y)}{\Delta\varphi(y) - \omega_0 D}, \quad (1.1)$$

where y is the coordinate in the field of view of the camera (see Fig. 1). In that relation, $\Delta\varphi(y)$ is the phase difference when the camera captures the intensity variations over a reference plane and over the surface of a two-dimensional (2D) object (the x direction is not considered) whose height h has to be determined. D is the distance between the projector and the camera and $\omega_0 \equiv \omega_p \cos \theta / G_p$, with ω_p as the frequency of the fringes on the projector's grating and G_p as the magnification factor of the projector (ω_0 is the frequency of the fringes on the projector

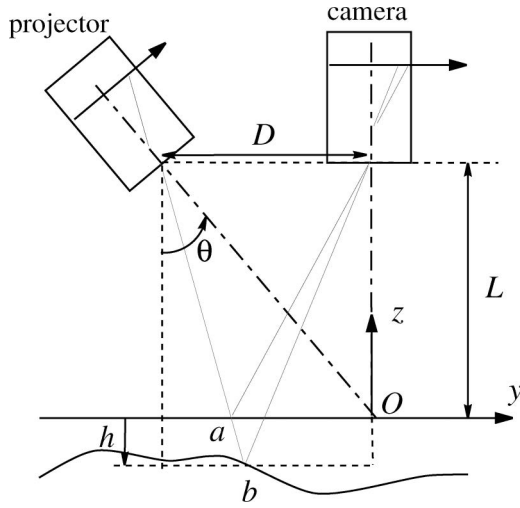


Fig. 1. Reproduction of Takeda's representation in crossed-optical-axes geometry. A fringe pattern is projected onto a reference surface (as point a) and on a deformed surface (point b). The corresponding phase variation in the intensity recorded by the camera is $\Delta\varphi(y)$ (2D object analysis is presented in Takeda's paper [2]).

image plane). Also, the derivation is performed assuming the camera and the projector that produces the intensity variations are at the same distance L from the reference plane.

In a very didactic paper, Rajoub *et al.* [17] have shown that this relation is incorrect. These authors propose a complete calculation relaxing the hypothesis that the camera and the projector are at the same distance from the reference plane. They propose an explanation of the error in Takeda's formula, which they attribute to an unjustified hypothesis of collimated projection. Also, in a previous paper [16], the same authors have derived the phase-to-height relation for collimated projection. Incidentally, note that these authors propose a relation between the height of the object h and the phase φ stored by the camera when capturing the intensity variations over the object surface, instead of using the usual phase difference $\Delta\varphi$.

Our paper follows from Rajoub's study. Our derivations concern both collimated and noncollimated projection for parallel- and crossed-optical-axes geometries. When we assume that the camera and the projector are at the same distance L from the reference plane, we find,

- for noncollimated projection in parallel-optical-axes geometry,

$$h(x', y') = \frac{L\Delta\varphi}{\Delta\varphi - \omega_0 D}, \quad (1.2)$$

where

$$x' = x - \frac{h}{L}x, \quad y' = y - \frac{h}{L}y; \quad (1.3)$$

- for noncollimated projection in crossed-optical-axes geometry,

$$h(x', y') = \frac{L\Delta\varphi(1 + \sin^2\theta y/D)^2}{\Delta\varphi(1 + \sin^2\theta y/D)[1 - \sin^2\theta(1 - y/D)] - \omega_0 D}; \quad (1.4)$$

- for collimated projection in parallel-optical-axes geometry,

$$h(x', y') = -\frac{L\Delta\varphi}{\omega_0 y}; \quad (1.5)$$

- for collimated projection in crossed-optical-axes geometry,

$$h(x', y') = \frac{L\Delta\varphi}{\omega \sin\theta(L - \cot\theta y)}. \quad (1.6)$$

In the above expressions, $\Delta\varphi$ stands for $\Delta\varphi(X', Y')$ or $\Delta\varphi(x, y)$, with (X', Y') and (x, y) being, respectively, the coordinates in the image plane of the camera and the coordinates in the field of view of the camera (thus $X' = -G_c x$ and $Y' = -G_c y$, with G_c the magnification factor of the camera).

Throughout this paper, we will compare our expressions in Eqs. (1.2), (1.3), (1.4), (1.5), and (1.6) with the expressions existing in the literature.

In this paper, we show experimental measurements performed using a calibrated object only in the case of noncollimated projection (Section 3). Our phase-to-height relations in Eqs. (1.2) and (1.4), together with Eq. (1.3), are shown to give a good determination of the object shape and the errors due to the use of Takeda's relation [Eq. (1.1)] are exemplified and discussed (Section 4).

The main contribution of our paper concerns noncollimated projection (as a consequence, the calculations concerning collimated projection are collected in Appendix B). On the one hand, we give a more tractable phase-to-height relation than that in [17], useful for direct application to real experiments. Notably, our Eqs. (1.2), (1.3), and (1.4) concern the phase difference $\Delta\varphi$ (instead of the absolute phase φ in [16,17]) that is known to compensate unwanted defects in the projection process [2]. In addition, we give experimental evidence of the validity of our expressions. On the other hand, we show that the error in Takeda's result is due to an erroneous manipulation of the phases φ (for projection on to the object) and φ_0 (for projection on to the reference plane). Otherwise, Takeda's calculations are correct. Our conclusion differs from Rajoub's argument, which implies an erroneous use of collimated projection.

Incidentally, some new results in our paper concern: the derivation of the varying fringe spacing in the crossed-optical-axes configuration and the derivation of the phase-to-height relation for collimated projection in the parallel-optical-axes geometry.

The paper is organized as follows: in Section 2, the phase-to-height relations are derived for

noncollimated projection. The cases of the parallel- and the crossed-optical-axes geometries are then considered as particular cases of this general result. The comparison with Takeda's relation is presented. Section 3 exemplifies our results with experimental data collected both in the parallel- and crossed-optical-axes configurations. A discussion on the obtained phases φ_0 and φ is presented, notably, the change in the fringe spacing in the crossed-optical-axes geometry (see also Appendix A). In Section 4, the derivation performed in Ref. [2] is analyzed and the error that leads to Eq. (1.1) is demonstrated. Finally, we collect in two appendices the derivation of the fringe spacing in the crossed-optical-axes geometry for noncollimated projection (Appendix A) and the derivation of the phase-to-height relations for collimated projection (Appendix B).

2. Derivation of the Phase-to-Height Relations

We consider the configuration of Fig. 2. With the only exception of this section, all the results presented in this paper concern the usual configuration, where the projector and the camera are at the same distance from the reference plane R (thus $L_p = L_c$).

In the following, we define the magnification factors for the projector G_p and for the camera G_c as for simple lenses with respective focal lengths f_p and f_c (positive magnification factors are considered, it being known that images through lenses are inverted): $G_p = L_p/(\cos \theta f_p)$ and $G_c = f_c/L_c$.

We also define ω_p as the fringe frequency in projector's grating (XY plane), $\omega = \omega_p/G_p$ as the fringe frequency in the image plane of the projector (I plane), and $\omega_c \equiv \omega/G_c$. We denote Σ as the surface whose height $h(x, y)$ with respect to the reference surface R is measured.

The image captured by the camera on the $(X'Y')$ plane is a pattern of gray levels corresponding to intensity variation $I(X', Y')$:

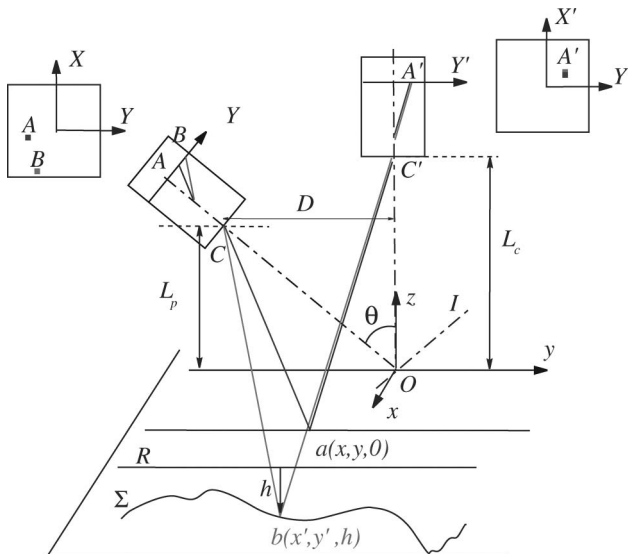


Fig. 2. Optical setup.

$$I(X', Y') = 1 + \cos \varphi(X', Y'). \quad (2.1)$$

When the fringes are projected onto the reference plane R , the intensity, or gray level, observed at point $A'(X', Y')$ is due to the ray AaA' , whose intensity is imposed by the intensity at the point A on the projector grating. Assuming a sinusoidal fringe projection (with the fringes oriented along the X axis), we have

$$\varphi_0(X', Y') = \omega_p Y_A. \quad (2.2)$$

For any reflecting surface Σ different from R , the intensity observed at point A' changes, because the ray arriving at A' is now the ray BbA' . This ray holds the intensity of the point B on the projector grating. Thus,

$$\varphi(X', Y') = \omega_p Y_B. \quad (2.3)$$

By definition, the phase difference $\Delta\varphi(X', Y') \equiv \varphi(X', Y') - \varphi_0(X', Y')$ is a measure of the change in intensity observed on A' .

Thus, the task is to determine the geometric relations between (X', Y') on the camera grating and Y_A or Y_B on the projector grating. The derivation is performed in the case of the ray BbA' , propagating from $B(X, Y)$ to $b(x', y', h)$ on any surface Σ and arriving at $A'(X', Y')$ to produce the phase $\varphi(X', Y')$. Then, $\varphi_0(X', Y')$ is deduced for R , being the reflecting surface (thus, $h = 0$).

To do that, we use the following geometric relations. On Fig. 3, we project, along the Ox axis in the plane $x = 0$, the rays Cb and bC' to produce Cb_0 and b_0C' with $b_0 = (0, y', h)$. The angles α and β measure, respectively, the angles $(\widehat{OCb_0})$ and $(\widehat{OC'b_0})$ in the plane $x = 0$. The angle $\theta = (\widehat{cCO})$ measures the inclination of the projector's axis with respect to the camera's axis.

Then, the angle α measures the position of the point B on the projector grating: $\tan \alpha = -Y_B/f_p$. On the other hand, in the triangle Ccb_0 , we have $\tan(\theta + \alpha) = (D + y')/(L_p - h)$. We get

$$\tan \alpha = -\frac{Y_B}{f_p} = \frac{(D + y') - \tan \theta (L_p - h)}{\tan \theta (D + y') + L_p - h}, \quad (2.4)$$

which is the first relation $Y_B(y')$. Then, the angle β is a measure of the position A' on the camera grating: $\tan \beta = -Y'/f_c$. In the triangle $C'c'b_0$, the angle β is involved as well and we get

$$\tan \beta = -\frac{Y'}{f_c} = \frac{y'}{L_c - h}. \quad (2.5)$$

This gives us the second relation, namely $y'(Y')$. Eliminating y' from the relations in Eqs. (2.4) and (2.5), we deduce $Y_B(Y')$:

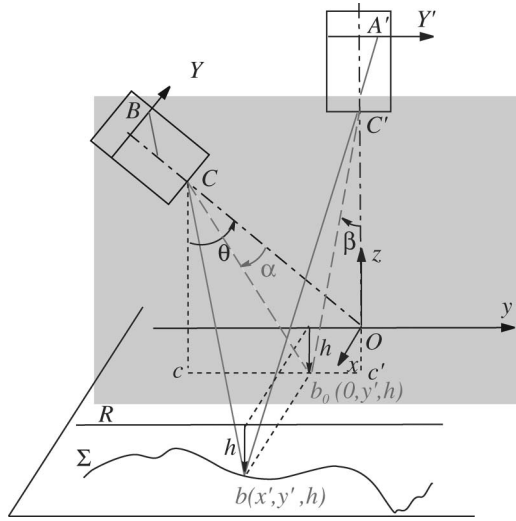
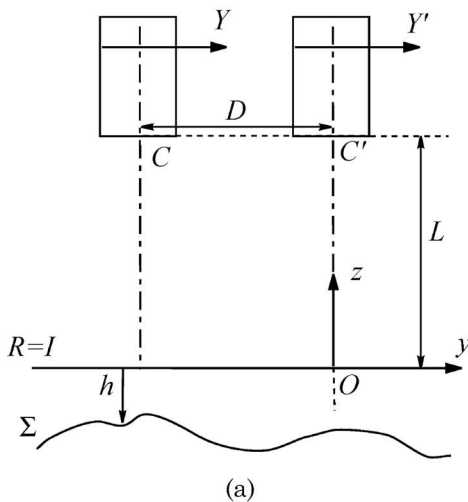


Fig. 3. In general, the rays Cb and bC' are not in a vertical plane. We define $b_0(0, y', h)$ as the projection of $b(x', y', h)$ in the plane $x = 0$ (which contains O , C , and C'). In this vertical plane $x = 0$, the angles α and β , respectively, measure $(\widehat{OCb_0})$ and $(\widehat{OC'b_0})$. These angles measure also the positions of B and A' on the projector and on the camera grating. The angle $\theta = (\widehat{CO})$ measures the inclination of the projector's axis with respect to the camera's axis.

$$Y_B = -f_p \frac{D - (L_c - h)Y'/f_c - \tan \theta (L_p - h)}{L_p - h + \tan \theta [D - (L_c - h)Y'/f_c]}, \quad (2.6)$$

and finally, the Eqs. (2.2) and (2.3) are

$$\begin{aligned} \varphi(X', Y') &= \frac{\omega_c}{\cos \theta (1 - h/L_p) - \tan \theta L_p^{-1} [(1 - h/L_c)Y'/G_c - D]} \\ &= \frac{\omega_c}{\cos \theta} \frac{(1 - h/L_c)Y' + G_c [(L_p - h) \tan \theta - D]}{(1 - h/L_p) - \tan \theta L_p^{-1} [(1 - h/L_c)Y'/G_c - D]}, \\ \varphi_0(X', Y') &= \frac{\omega_c}{\cos \theta} \frac{Y' + G_c [L_p \tan \theta - D]}{1 - \tan \theta L_p^{-1} [Y'/G_c - D]}. \end{aligned} \quad (2.7)$$



The above relation for $\varphi(X', Y')$ is in agreement with Rajoub's result, Eq. (36) in [17] (see also the note in [18]).

To conform with most of the literature, we express φ as a function of (x, y) owing to $x = -X'/G_c$, $y = -Y'/G_c$:

$$\begin{aligned} \varphi(x, y) &= -\frac{\omega}{\cos \theta} \frac{y - L_p \tan \theta + D + h/L_c (L_c \tan \theta - y)}{1 + \tan \theta (D + y)/L_p - h/L_p (1 + \tan \theta y/L_c)}, \\ \varphi_0(x, y) &= -\frac{\omega}{\cos \theta} \frac{y - L_p \tan \theta + D}{1 + \tan \theta (D + y)/L_p}. \end{aligned} \quad (2.8)$$

Finally, it is important to note that the shift in the position is given by $\delta x \equiv x' - x$ and $\delta y \equiv y' - y$, since the height h is measured at (x', y') and not at (x, y) . The shift in y is directly obtained from $\tan \beta = y/L_c = y'/(L_c - h)$. The shift in x is easily obtained by using the property that the ray bC' coincides with the ray aC' (Fig. 3 and see the note in [19]). We get

$$x' = x - \frac{h}{L_c} x, \quad y' = y - \frac{h}{L_c} y, \quad (2.9)$$

with $h = h(x', y')$.

In the following, we inspect the case of the usual configurations of parallel- and crossed-optical-axes geometry. Also, we consider now $L = L_c = L_p$ (Fig. 4).

A. Parallel-Optical-Axes Geometry

This case Fig. 4(a) is deduced from the preceding relations in Eq. (2.8) with $L = L_c = L_p$ and $\theta = 0$, leading to

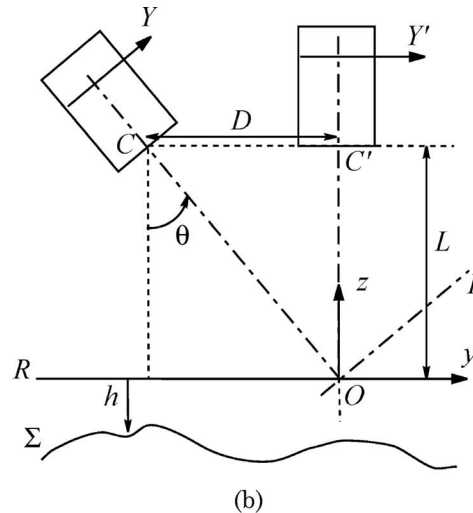


Fig. 4. Optical setup for the projector and the camera at the same distance L from the reference plane R , (a) in the parallel- and (b) in the crossed-optical-axes geometries.

$$\Delta\varphi(x,y) = -\omega_0 \frac{Dh(x',y')}{(1 + \sin^2\theta y/D)[1 + \sin^2\theta y/D - h(x',y')/L(1 - \sin^2\theta(1 - y/D))]}, \quad (2.14)$$

$$\begin{aligned} \varphi(x,y) &= -\omega y - \omega D \frac{L}{L - h(x',y')}, \\ \varphi_0(x,y) &= -\omega y - \omega D. \end{aligned} \quad (2.10)$$

Thus,

$$\Delta\varphi(x,y) = -\omega D \frac{h(x',y')}{L - h(x',y')}. \quad (2.11)$$

This relation is in agreement with the relation derived by Takeda (Eq. (1.1) with $\omega_0 = \omega$ here). However, the h value is measured at the (x',y') position, not at the (x,y) position, as assumed by Takeda. This shift in the position is $(\delta x = x' - x = -h/Lx, \delta y = y' - y = -h/Ly)$. Experimental evidence of this discrepancy is presented in Subsection 3.C.

As expected in that configuration, $\varphi_0(x,y)$ is p periodic along y ($p = 2\pi/\omega$) since the image plane of the projector I and the object plane of the camera R coincide.

B. Crossed-Optical-Axes Geometry

In that case [Fig. 4(b)], the relations in Eq. (2.8) are used owing to $L = L_c = L_p$ and $\tan\theta = D/L$. We get

$$\begin{aligned} \varphi(x,y) &= -\omega \cos\theta \\ &\times \frac{y + h(x',y')/L(D-y)}{1 + \sin^2\theta y/D - h(x',y')/L[1 - \sin^2\theta(1 - y/D)]}, \\ \varphi_0(x,y) &= -\omega \cos\theta \frac{y}{1 + \sin^2\theta y/D}. \end{aligned} \quad (2.12)$$

As expected, $\varphi_0(x,y)$ is not periodic along y since the image plane of the projector I and the object plane of the camera R do not coincide. Note that the expression of $\varphi_0(x,y)$ in Eq. (2.12) differs from the usually cited relation for the varying frequency $f(y) \equiv \varphi_0(x,y)/(2\pi y)$ when fringe pattern is projected on the reference plane [12,13,20]:

$$\varphi_{0S}(x,y) = -\omega \cos\theta [1 - 2\sin\theta \cos\theta y/L]. \quad (2.13)$$

This error has been analyzed in [17] and it can be seen here that the expression is not valid, even in the approximation $y/L \ll 1$, as used in [20]. Experimental evidence of this error is shown in the forthcoming Fig. 8, Section 3. We get

where we have defined, following Takeda's notation, $\omega_0 \equiv \omega \cos\theta$ ($p_0 = 2\pi/\omega_0$ is the periodicity of the fringes when projected in the image plane I of the projector).

The relation between the measured unwrapped phase distribution $\Delta\varphi$ to the object height h in Eq. (2.14) clearly differs from Takeda's relation

$$\Delta\varphi_T(x,y) = -\omega_0 \frac{Dh(x,y)}{L - h(x,y)}. \quad (2.15)$$

The source of the error in Takeda's derivation is discussed in Section 4 and exemplified in Subsection 3.C. However, many studies using Takeda's law have obtained good results [5,6,12,13], suggesting that the error might be negligible. It is easy to see that

$$\Delta\varphi = \Delta\varphi_T \mathcal{C}(\theta, h/L, y/D), \quad (2.16)$$

where

$$\begin{aligned} \mathcal{C}(\theta, h/L, y/D) &= \left[1 + \sin^2\theta \left(\frac{y}{D} - \frac{h}{L-h} \right) \right]^{-1} \\ &\times \left[1 + \sin^2\theta \frac{y}{D} \right]^{-1}. \end{aligned} \quad (2.17)$$

The function $\mathcal{C} \sim 1$ for (i) the angle $\theta \ll 1$ and (ii) $h/L \ll 1$, $y/D \ll 1$. These conditions are often fulfilled in the referenced studies: for instance, $\theta \sim 0.19$ rad, $h/L \sim 0.07$, and $y/D \sim 0.3$ in [14], or $\theta \sim 0.3$ rad, $h/L \sim 0.0045$, and $y/D \sim 0.2$ in [6]. This explains the agreement with Takeda's law presented in the literature. To summarize, the error in Takeda's law is

$$\Delta\varphi = \Delta\varphi_T [1 + O(\theta^2 h/L, \theta^2 y/D)]. \quad (2.18)$$

However, it is now evident that this error proves to be very important in the case of short-range profilometry, where $h/L \sim 1$, and in large-field profilometry, in which the object's size is comparable to the camera-projector distance.

3. Experimental Results

In this section, we inspect experimentally the reconstruction of h on the basis of Eqs. (2.11) and (2.14) together with Eq. (2.9). To do that, we carried out the following experiment. The measured object is a triangular prism with base line 6 cm and height 3 cm. The prism is placed on the reference plane R (Fig. 5) at a distance y_0 of the camera axis (the triangle is symmetric with respect to the $y = y_0$ axis).

Thus, the surface Σ differs from the reference plane R only in a region $-3 \text{ cm} < y - y_0 < 3 \text{ cm}$, hereafter referred to as the T region. The height $h(x, y)$ is invariant along the x direction, perpendicular to the plane of Fig. 5. Otherwise, $L = 105.2 \text{ cm}$, θ can vary, and, for $\theta = 0$ (parallel-optical-axes configuration), we have $D = 18 \text{ cm}$.

A sinusoidal fringe pattern is projected onto the object and a CCD camera is used to record the deformed fringe of the object. Details on the optical devices are given below; afterward, the results are presented and analyzed.

A. Optical Devices

Fringe-pattern projection is achieved by means of a computer-controlled digital videoprojector with a high resolution of $1920 \text{ pixels} \times 1080 \text{ pixels}$ and 12 bit depth per color. An important improvement arising from the use of a digital video projector is that we are able to project sinusoidal fringe patterns with a controlled wavelength. Usually, the projected pattern is a square profile (Ronchi grating), extremely unadapted for Fourier analysis. Indeed, the use of a sinusoidal grating strongly increases the quality of the filtering process as well as the phase recovering. Another important improvement with a video projector compared to a slide-projector usually employed is that a video projector can project an image on a surface shifted with respect to its axis and, hence, more centered to the camera axis. The video projector allows a correction of the projected image so that the image is not distorted and keeps the fringes' wavelength constant all over the image and maintains the original sharpness. However, due to the fact that the projected pattern varies discretely in space and is digitized in intensity, the video projector's resolution is lower than that of a slide projector.

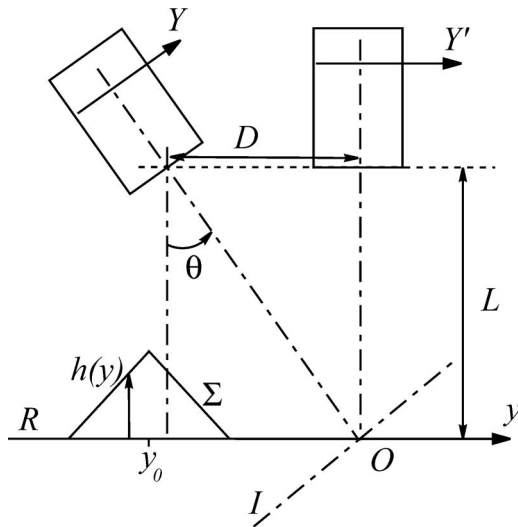


Fig. 5. Experimental configuration: Σ is at distance $h(y)$ from the reference plane R with $h(0 < y - y_0 \leq -3 \text{ cm}) = y$, $h(0 < y - y_0 \leq 3 \text{ cm}) = -y$ zero, otherwise. I is the image plane of the projector. In the experiments, $L = 105.2 \text{ cm}$ and θ can vary, and for $\theta = 0^\circ$ (parallel-optical-axes geometry), $D = 18 \text{ cm}$.

For a given projection distance, the size of the projected optical field can be adjusted (by means of the projector zoom optics) to cover either a small or a relatively large area of the surface. In particular, we employed a projection distance of $L = 1 \text{ m}$, which allowed us to work with projection windows of sizes ranging from approximately $36 \text{ cm} \times 20 \text{ cm}$ to $80 \text{ cm} \times 45 \text{ cm}$.

The fringe patterns projected onto the object were recorded by a Fujifilm Finepix S2 Pro SRL-type digital still camera, with a $3024 \text{ pixel} \times 2016 \text{ pixel}$ CCD and a color depth of 16 bits per color. To avoid any artifact from the camera's preprocessing algorithm (such as those coming from quantization, compression, color depth reduction, etc.) we worked with raw images that were later developed into portable pixmap (PPM) format at full color depth.

The whole fringe-projection and image-capturing system is held over the channel, supported by a mobile structure that allows for precise alignment and repositioning of the optical devices. The whole setup has been tested and validated in a previous study [21].

B. Intensity Variations Captured by the Camera

Figures 6 show the intensity variations $I(x, y)$ on the surface Σ recorded by the camera (as previously said, h and thus I are invariant along the x direction). The cases of the parallel- and the crossed-optical-axes geometries (with $\theta = 33.9^\circ$, thus $D = 70.7 \text{ cm}$ in that case) are shown. Figure 7 shows the corresponding curves $I(y)$, averaged over the x direction.

Several remarks can be made regarding these figures. In the case of parallel optical axes, the T region, where a change in height occurs, is well resolved on both sides. Outside of this region, the fringes are regularly spaced (with period $p \simeq 0.27 \text{ cm}$ invariant from left to right). In the T region, h linearly increases for $-3 \text{ cm} < y < 0$ and then linearly decreases for $0 < y < 3 \text{ cm}$. From the expression of $\varphi(x, y)$ in Eq. (2.10), it is easy to see that $h = ay$ leads to an apparent frequency $\omega_a \simeq \omega(1 + aD/L)$ and fringe spacing of $p_a \simeq p/(1 + aD/L)$. In our experiments, $a = \pm 1$ and $D/L = 0.171$ give $p_a = 0.24 \text{ cm}$ and $p_a = 0.34 \text{ cm}$ as observed in Figs. 6(a) and 7(a) (see also Appendix A).

In the crossed-optical-axes geometry (here, for $\theta = 33.9^\circ$), the T region is badly resolved for $0 < y < 3 \text{ cm}$ because of the projected shadow. Outside of this region, the fringes are not regularly spaced because the image plane I of the projector does not coincide with the reference plane. The fringe spacing varies from roughly 0.35 to 0.4 cm from left to right. This increase in the spacing p_n ($n = 0$ at the origin O) is as expected: $p_n = p_I / \cos \theta [1 - n \sin \theta p' / L] - 1 [1 - (n - 1) \sin \theta p_I / L]^{-1}$, where p_I is the fringe spacing observed on the image plane of the projector I (see Appendix A). Here, p_I can be deduced from p owing to the invariant $p_p / f_p = p / L = p_I \cos \theta / L$; thus, $p_I \simeq 0.325 \text{ cm}$. Finally, as in the parallel-optical-axes geometry, a successive decrease and increase in the fringe spacing is observed in the T region. From Eq. (2.12), $p_a \simeq p_I / [\cos \theta (1 + a \tan \theta)]$ gives

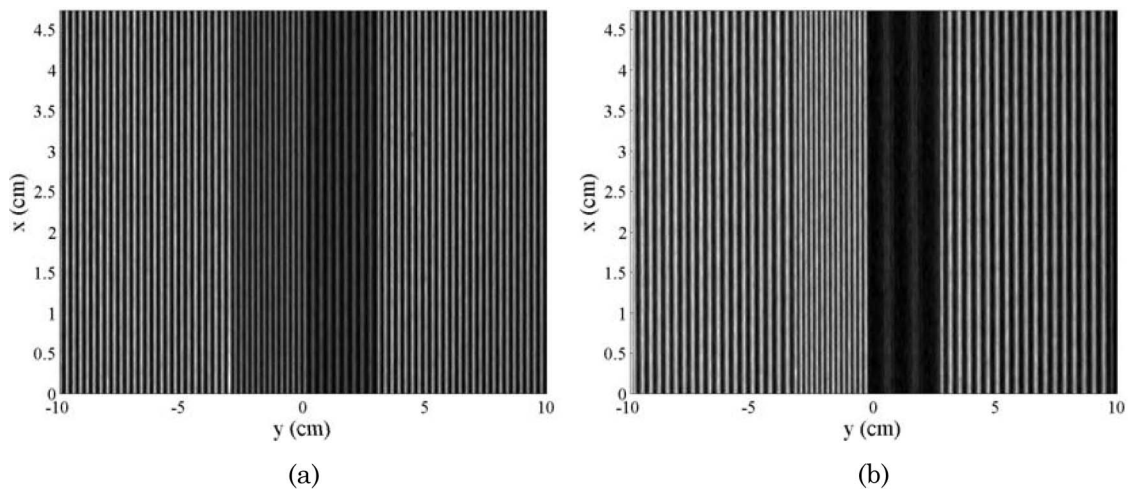


Fig. 6. Experimental intensity variations $I(x,y)$ captured by the camera (a) in the parallel-optical-axes geometry with $D = 18$ cm and $L = 105.2$ cm and (b) in the crossed-optical-axes geometry with $D = 70.7$ cm ($\theta = 33.9^\circ$), $L = 105.2$ cm, and $y_0 = 0$.

$p_a = 0.23$ cm and $p_a = 1.19$ cm. The agreement is good (see the Appendix A). Finally, Fig. 8 shows the unwrapped phase $\varphi_0(y)$ (see [22]) deduced from $I_0(y)$ when projected onto the reference plane in the absence of the triangle ($I_0(y)$ corresponds to the average of $I_0(x,y)$ in the x direction). It can be seen that our expression in Eq. (2.12) accurately fits the experimental points while the expression given in [12,13,20] [see Eq. (2.13)] significantly fails to reproduce the data.

C. Phase-to-Height Inversion

In this section, from the experimental curves of $I_0(y)$ and $I(y)$, we deduced the unwrapped phase difference $\Delta\varphi(y)$. Then, we use the inversion of Eqs. (2.11) and (2.14) together with Eq. (2.9) to get the height $h(y)$. The comparison with Takeda's law is presented.

1. Parallel-Optical-Axes Geometry

Figures 9 illustrate the phase-to-height inversion (the additional dependence of $\Delta\varphi(y)$ on x is omitted because of the aforementioned invariance along x in

our experiments): from $I(y)$ and $I_0(y)$ [Fig. 9(a)], we extract the phase difference $\Delta\varphi(y)$. This is done by filtering the 2D Fourier transform of $I(I_0)$ around the main frequency ω (in the present case, a simple Gaussian filter of width $\omega/2$ is used). The inverse Fourier transform is a complex signal whose unwrapped phase is $\varphi(y)$ (correspondingly, $\varphi_0(y)$), and then $\Delta\varphi = \varphi - \varphi_0$ [Fig. 9(b)]. In the parallel-optical-axes geometry, the inversion of $\Delta\varphi(y)$ gives, both in our approach and in Takeda's approach,

$$h(y') = \frac{L\Delta\varphi(y)}{\Delta\varphi(y) - \omega_0 D}, \quad (3.1)$$

with $y' = y + \delta y$ and $\delta y = -yh/L$. Figure 9(c) shows the reconstructed height; here the shift in position δy is visible: $\Delta\varphi$ reaches its extremum at $y \sim -25$ cm while h reaches its maximum at $y = y_0 = -24$ cm. The agreement between the reconstructed shape and the real shape is good, very comparable to the results obtained in a similar experiments [10].

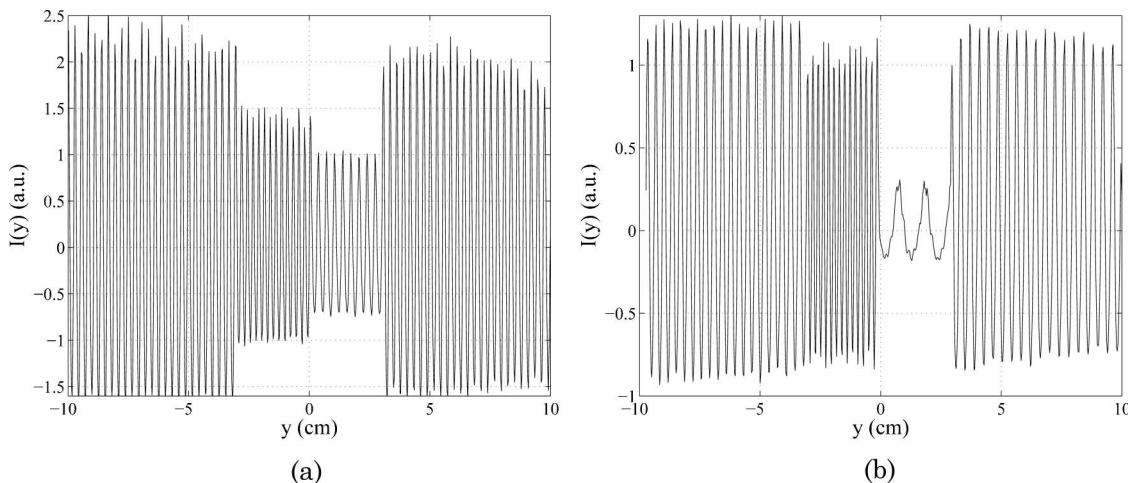


Fig. 7. Intensity variations $I(y)$ in (a) the parallel- and (b) the crossed-optical-axes geometries. The curves correspond to the averages over the x direction of the 3D plot in Fig. 6.

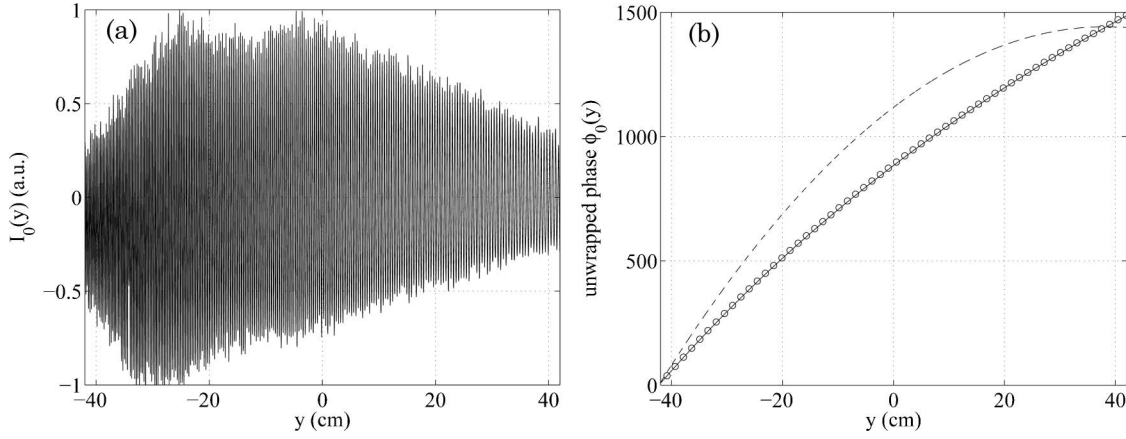


Fig. 8. (a) Intensity variations $I_0(y)$ for fringe projection onto the reference plane in the absence of the triangular prism and (b) the corresponding unwrapped phase $\phi_0(y)$ (see [23]). Experiments correspond to $\theta = 33.9^\circ$ with $L = 105.2$ cm. The points are the experimental data (only one point of each 150 points is indicated for visibility), the solid curve corresponds to our Eq. (2.12) and the dashed curve corresponds to Eq. 2.13 from [12,13,20].

The error in Takeda's approach consists of neglecting the spatial shift of the sampling points introduced by the object's height profile.

Figure 10 presents a comparison between the reconstructed heights h and h_T , obtained using Eq. (3.1), including or omitting, respectively, the shift δy for various y_0 values. As expected, the error in h_T increases when y_0 increases. The maximum error in the shift is $\delta y_{\max} = y_0 h_{\max}/L$ (thus, a constant relative error $\delta y/y_0 = h_{\max}/L = 2.85\%$), which leads to, for $y_0 = -8$ cm, $\delta y_{\max} = 0.23$ (0.2 experimentally obtained); for $y_0 = -16$ cm, $\delta y_{\max} = 0.456$ (0.4 experimentally obtained); and, for $y_0 = -24$ cm, $\delta y_{\max} = 0.684$ (0.66 experimentally obtained).

2. Crossed-Optical-Axes Geometry

The same experiments have been performed in the crossed-optical-axes geometry. In that case, the inversion is, from Eq. (2.14),

$$h(y') = \frac{L\Delta\phi(y)(1 + \sin^2\theta y)^2}{\Delta\phi(y)(1 + \sin^2\theta y/D)[1 - \sin^2\theta(1 - y/D)] - \omega_0 D}. \quad (3.2)$$

The position of the triangular prism y_0 and the angle between the optical axes θ have been varied. The procedure to derive $\Delta\phi(y)$ is the same as in the parallel-

optical-axes geometry, but a wider filter has been used (of width around ω) to account for the change in the frequency in the nonperiodic signal. The peak in the Fourier transform corresponds in that case to the mean fringe periodicity. Figure 11(a) shows the results obtained varying y_0 for $\theta = 33.9^\circ$ and Fig. 11(b) shows the results obtained varying θ for $y_0 = -16$ cm. Both figures exemplify the error due to the use of Takeda's result, while our present inversion gives a good height reconstruction. Note that Takeda's expression of the height h_T in Eq. (1.1) is given as a function of h by

$$h_T(y) = \frac{h(y')}{A^2 + (AB + h(y'))h(y')/L}, \quad (3.3)$$

with $A \equiv 1 + \sin^2\theta y/D$ and $B \equiv \cos^2\theta - \sin^2\theta y/D$.

4. On Takeda's Calculation

In [16], it is said that Takeda's approach uses an unjustified hypothesis of collimated projection. We will show that this is not the case. Actually, the expressions of the phases ϕ and ϕ_0 are correct in [2] but an erroneous subtraction of the two phases leads to an error in the phase difference.

Let us recall the meaning of the phase difference ϕ : it corresponds to the change in intensity at a given

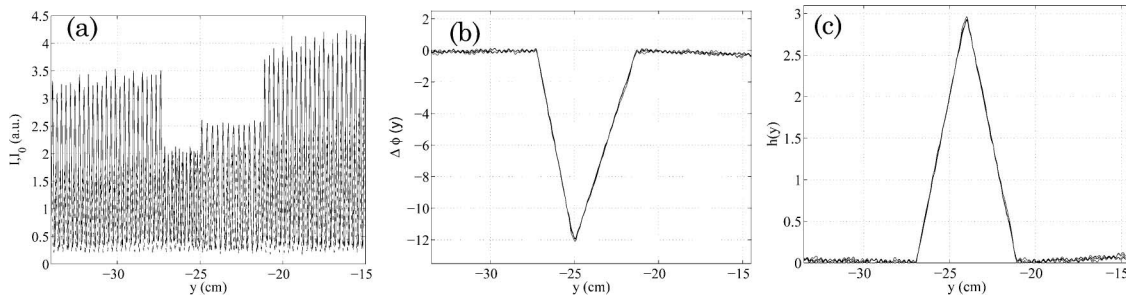


Fig. 9. (a) Signals $I_0(y)$ and $I(y)$ for fringe projections on the reference plane R and on the Σ plane. (b) Unwrapped phase difference $\Delta\phi(y)$ and (c) reconstructed height $h(y)$ using Eqs. (2.9) and (2.11). The experiment is conducted in the parallel-optical-axes geometry with $L = 105.2$ cm, $D = 18$ cm, and $y_0 = -24$ cm.

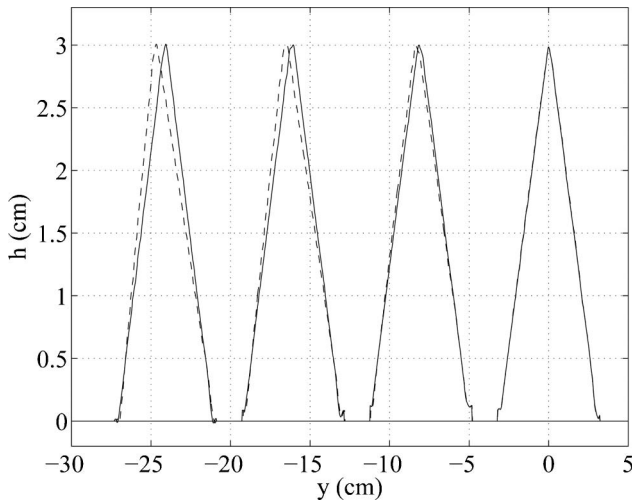
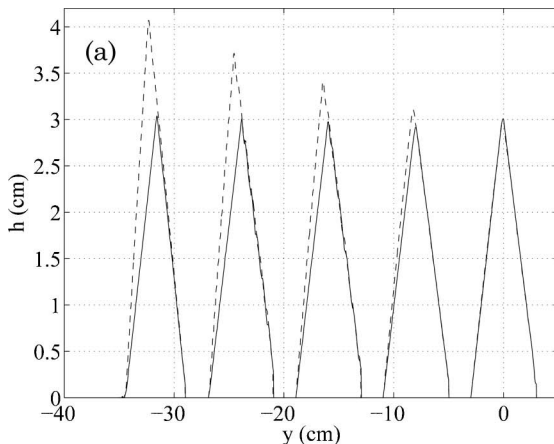


Fig. 10. Height reconstruction $h(y)$ for various y_0 values. Solid curves correspond to our phase-to-height relation and dashed curves correspond to Takeda's phase-to-height relation. The experimental configuration is the same as in Fig. 9.

pixel of the camera (A' in Fig. 2) for a change in the reflecting surface (say R and Σ). The intensity at this pixel changes because the rays arriving at A' come from two different points of the projector grating (A and B in Fig. 2).

Takeda's geometrical representation [reproduced in Fig. 12(a), for reference] is different from our Fig. 2. Two rays coming from the same point B of the projector grating are considered: the ray BaA' for a reflecting surface being R and the ray BbB' for a reflecting surface being Σ . Of course, these two rays produce the same intensity, either on A' or on B' in the camera. When R is the reflecting surface, the ray BA' is seen as coming from a on R , when Σ is the reflecting surface, the ray BB' is seen as coming from b_a on R [Fig. 12(b)]. Again, the two rays hold the same intensity:

$$\varphi = \omega_p Y_B. \quad (4.1)$$



Following Takeda, geometric considerations allow expressing the phases φ_0 and φ . First, from Figs. 12, $X_B = (f_p \cos \theta / L) \overline{Ob'}$, with b' as the point intercepting I along the ray Bb . Thus, we have $\varphi = \omega \overline{Ob'}$, where $\omega = \omega_p / G_p$ is the frequency of the fringes on the plane I (the fringes are regularly spaced on that plane). We can now define $\omega_0 = \omega \cos \theta$ as in Takeda's paper and we get, introducing b_a as the point intercepting R along the ray bB' ,

$$\varphi = \omega \overline{Ob'} = \omega_0 \overline{Ob_a} + \omega_0 \left(\frac{\overline{Ob'}}{\cos \theta} - \overline{Ob_a} \right). \quad (4.2)$$

The point b_0 is the point intercepting R with $b'b_0$ parallel to the projector's axis CO . It is sufficient to remark that $\overline{Ob_0} = \overline{Ob'}/\cos \theta$ (since the triangle Ob_0b' is a rectangle at b' by construction of the point b_0). We deduce, as Takeda,

$$\varphi(y) = \omega_0 y + \omega_0 \overline{b_a b_0}, \quad (4.3)$$

where it has been implicitly defined that $y = \overline{Ob_a}$.

The following step in Takeda's approach is to consider the same ray coming from B when the reflecting surface is R (the Oy plane). In that case, the ray is reflected on R at point a . The same geometric considerations can be done: we have $a' = b'$ and $a_0 = b_0$ because the ray Ba used to define a' and a_0 is the same as the ray Bb , and we have $a_a = a$. We get

$$\varphi_0(y') = \omega_0 y' + \omega_0 \overline{ab_0}, \quad (4.4)$$

but here, $y' = \overline{Oa}$.

Both expressions in Eqs. (4.3) and (4.4) are correct. The error in Takeda's approach is to build $\Delta\varphi(y)$ from the difference between both expressions, considering $y' = y$: Takeda's phase difference is $\Delta\varphi_T(y) = \varphi(y' = y) - \varphi_0(y)$. This erroneous subtraction gives

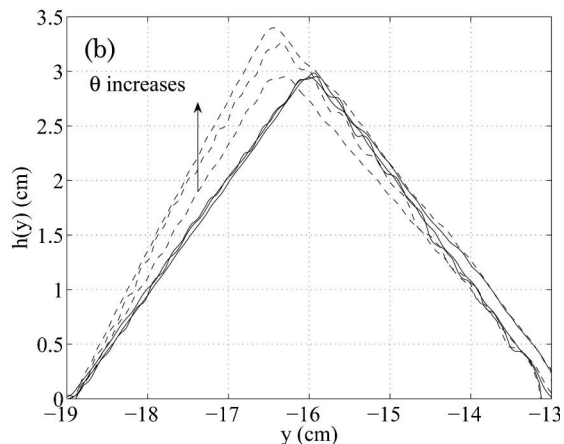


Fig. 11. Reconstructed height $h(y)$ in the crossed-optical-axes geometry (a) for $\theta = 33.9^\circ$ and varying the y_0 position of the triangle and (b) for $y_0 = -16$ cm and varying $\theta = 0, 18.1$ and 41° . Solid curves correspond to our height reconstruction from Eq. (3.3) with Eq. (1.2). Dashed curves are the height reconstructed using Takeda's relation Eq. (1.1).

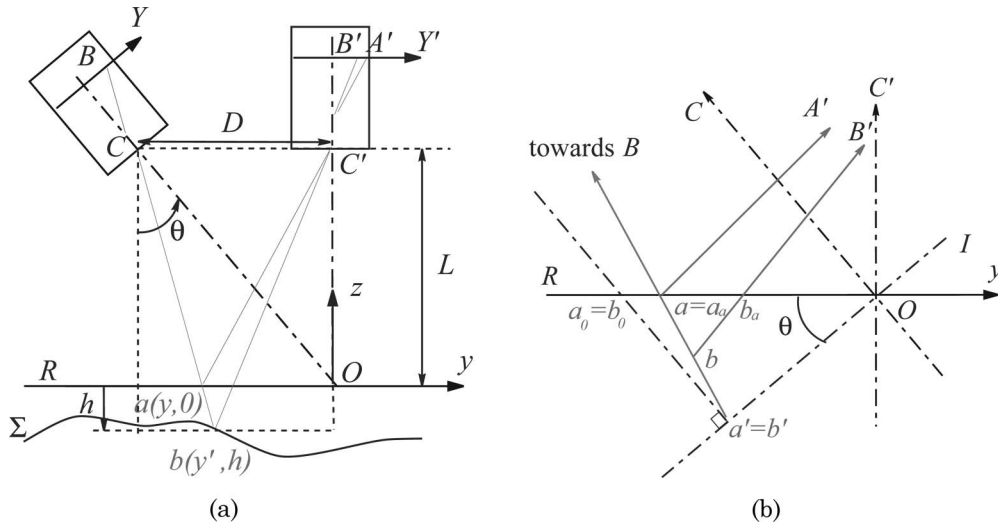


Fig. 12. (a) Reproduction of Takeda's representation and (b) the same representation including useful additional points: b' is the point of the ray Bb on the plane I , b_a is the point of ray bB' on the plane $R(Oy)$, and b_0 is the point on plane R with b_0b' parallel to the projector's optical axis CO . Similar construction is used to define a_a , a_0 , and a' .

$$\Delta\varphi_T(y) = \omega_0 \overline{b_a a} = -\omega_0 \frac{hD}{L-h}. \quad (4.5)$$

When considering the correct definitions of y and y' , the terms $\omega_0(y' - y)$ remain (with $y = \overline{Ob_a}$ and $y' = \overline{Oa}$) and we get

$$\Delta\varphi = \omega_0(\overline{Ob_a} - \overline{Oa}) + \omega_0(\overline{b_a b_0} - \overline{ab_0}) = 0, \quad (4.6)$$

which is expected, since the two rays hold the same intensity !

However, with $\varphi_0(y)$ and $\varphi(y')$ being correctly derived, it is easy to correct the last erroneous operation. We keep the same expression for $\varphi(y)$ (the ray is BbB'). To derive φ_0 , we consider the ray AaB' , with $a = b_a$ that is seen by the camera as coming from b_a , as illustrated on Fig. 13. We have $Y_A/f_p = \overline{Oa'} \cos \theta / L$, but now, a' differs from b' (and $a_0 \neq b_0$). We have now a unique definition of $y = \overline{Ob_a} = \overline{Oa}$ and

$$\varphi(y) = \omega_0 y + \omega_0 \overline{ab_0}, \quad (4.7)$$

$$\varphi_0(y) = \omega_0 y + \omega_0 \overline{aa_0}, \quad (4.8)$$

from which we deduce

$$\Delta\varphi(y) = \omega_0 \overline{aa_0}. \quad (4.9)$$

This expression is correct and equivalent to our expression in Eq. (2.11) for $\theta = 0$ and to our expression in Eq. (2.14) for $D = L \tan \theta$ (see the note in [23]).

5. Concluding Remarks

We have inspected the 3D phase-to-height relationship used in fringe-projection profilometry in the cases of collimated and noncollimated projection. In the past ten years, the need for performing accurate noncontact measurements has motivated studies on signal processing, such as unwrapping phase algorithms [5,14,15] or filtering techniques [8–11]. The goal is to enhance the quality of the height reconstruction in these methods. Thus, it is important that the basic phase-to-height relation is exact (at least in the geometric optics approximation). We have confirmed the relation first given by Rajoub *et al.* [17] and we have given experimental evidence of this analytical prediction. Also, the error due to the usually cited phase-to-height relation in Eq. (1.1) is explained and experimentally exemplified.

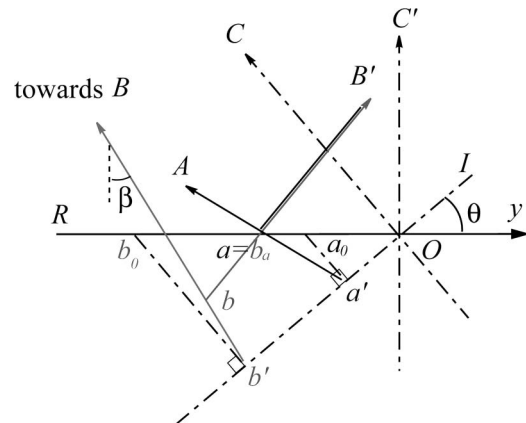


Fig. 13. Same representation as in Fig. 12(b) considering the ray AaB' instead of the ray BaA' . Now the ray AB' is seen by the camera as coming from point $a = b_a$. Otherwise, the same definitions for the points a' , b' and a_0 , b_0 as in Fig. 12(b) are used.

Appendix A: On the Fringe Spacing in Crossed-Optical-Axes Geometry

The object of this appendix is to derive Eq. (A5), which gives the change in the fringe spacing on the reference plane R in the crossed-optical-axes geometry.

We report in Fig. 14 the figure used in [17]. On the projector grating, we consider the rays r_n with $2n\pi$ phase difference with the ray CO . r_n forms an angle α_n with CO . The two successive rays r_n and r_{n+1} have 2π phase difference.

The conjugate image of the projector's grating is formed on the plane I , with a regular spacing p_I , and we denote w_n as the point of r_n on I .

The fringe spacing on the reference plane R varies along y and we denote $p_{n+1} \equiv y_{n+1} - y_n$ with y_n as the point of r_n on R . The aim of this appendix is to derive p_n .

On I , we have

$$\tan \alpha_n = \frac{\overline{Ow_n}}{L/\cos \theta}, \quad \overline{Ow_n} = np_I, \quad (\text{A1})$$

where the last relation is drawn from the fact that I is the conjugate plane of the projector image plane. On R , we have

$$\tan(\theta + \alpha_n) = \frac{\overline{C'y_n}}{L}. \quad (\text{A2})$$

With $\overline{C'y_n} = L \tan \theta + y_n$, we get

$$p_{n+1} = L[\tan(\theta + \alpha_{n+1}) - \tan(\theta + \alpha_n)], \quad (\text{A3})$$

which simplifies in

$$p_{n+1} = \frac{L}{\cos^2 \theta} \frac{\tan \alpha_{n+1} - \tan \alpha_n}{(1 - \tan \theta \tan \alpha_n)(1 - \tan \theta \tan \alpha_{n+1})}. \quad (\text{A4})$$

With $\tan \alpha_n = np_I \cos \theta / L$ from Eq. (A1), we get

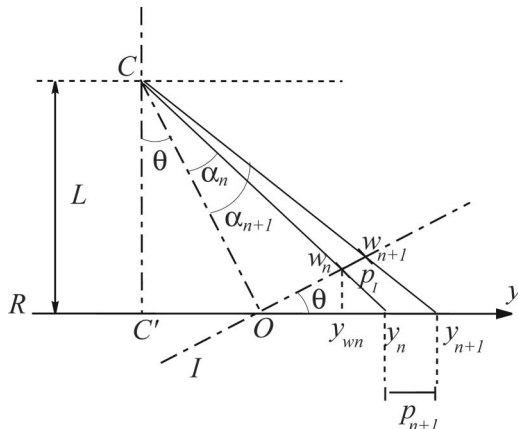


Fig. 14. System geometry used to calculate the fringe spacing p_n in the crossed-optical-axes geometry.

$$p_{n+1} = \frac{p_I}{\cos \theta} \frac{1}{(1 - n \sin \theta p_I / L)[1 - (n + 1) \sin \theta p_I / L]}. \quad (\text{A5})$$

The above formula is exact and can be easily calculated in practice.

From our experimental configuration described in Subsection 3.B, we can deduce the fringe spacing p_I on I from the fringe spacing p obtained in the parallel-optical-axes configuration: $p_I = p / \cos \theta$. We have $p \simeq 0.27$ cm from Fig. 7(b) outside the T region; thus, $p_I \simeq 0.325$ cm. Then, p_n is calculated from Eq. (A5). Figure 15 shows the fringe spacing experimentally deduced from Fig. 7, both in the parallel- and in the crossed-optical-axes geometries. The apparent frequency is given as well in the T region (for a linear increase or decrease of the height $h(y)$ with slopes ± 1). In the parallel-optical-axes geometry, $p_a \simeq p / (1 \pm D/L)$ (in the referred experiments, $D = 18$ cm and $L = 105.2$ cm) and, in the crossed-optical-axes geometry, $p'_a \simeq p_I / [\cos \theta (1 \pm \tan \theta)]$ (in the referred experiments, $\theta = 33.9^\circ$). Note that a reasonable fit of the experimental data are obtained in the crossed-optical-axes geometry using $p_I \sim 0.313$ cm, suggesting an error of around 3% either in the angle θ or in the position of the plane I .

Rajoub *et al.* [17] show that the derivation of p_n in [20] is inexact and propose the approximate expression (Eq. (20) in [17]). Unfortunately, their derivation contains a mistake from his Eq. (15) to Eq. (16), where they have used $w_n = y_{w_n} \cos \theta$ instead of using $w_n = y_{w_n} / \cos \theta$. Owing to this correction, we get a modified version of his Eq. (20) (replacing simply y_{w_n} by $y_{w_n} / \cos^2 \theta$):

$$p_n \simeq \frac{p_0}{\cos \theta} \frac{1 + \sin \theta \cos \theta y_{n+1} / L}{1 - \tan \theta y_{w_n} / L}, \quad (\text{A6})$$

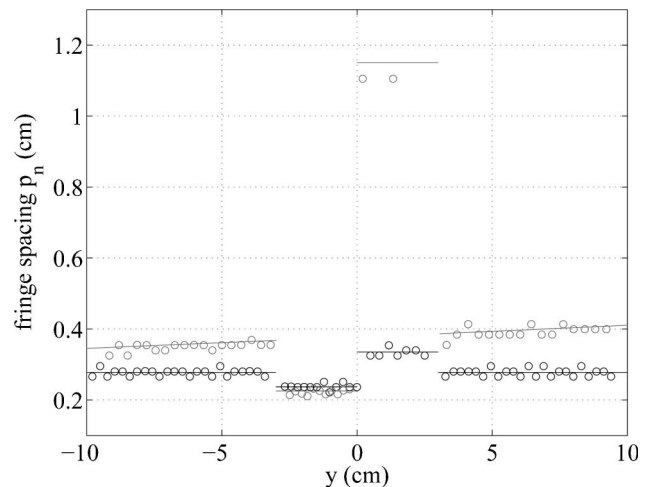


Fig. 15. Open circles, experimental fringe spacing deduced from Fig. 7 in the parallel- and the crossed-optical-axes geometries (the crossed-axes geometry gives higher fringe spacing). The solid curves correspond to our expression in Eq. (A5) and in the body of the text.

where it has been assumed that the linear dimension of the illuminated area, Ow_{n+1} , is small compared to the projection distance $L/\cos\theta$, thus, α_n is small. Rajoub concludes, however, that the above expression contains two unknowns y_{n+1} and y_{w_n} . They are actually known; owing to $y_{n+1} = L[\tan(\theta + \alpha_{n+1}) - \tan\theta]$ and $y_{w_n} = np_0 \cos\theta$ (the triangle $Ow_n y_{w_n}$ is rectangle at y_{w_n}), we get

$$p_n \simeq \frac{p_0}{\cos\theta} \frac{1 + \sin\theta \cos\theta [\tan(\theta + \alpha_{n+1}) - \tan\theta]}{1 - \sin\theta \cos\theta np_0/L}, \quad (\text{A7})$$

which simplifies exactly in the same expression as our Eq. (A1) (suggesting that the assumption of small α_n angles is not necessary in [17]).

Appendix B: The Case of Collimated Projection

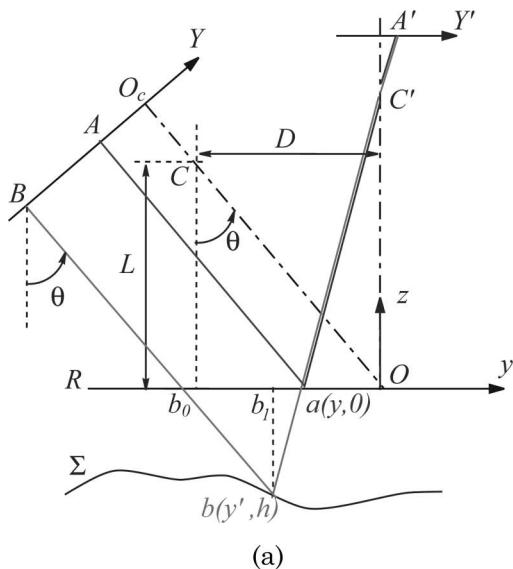
In this appendix, we derive the expression of the phase difference $\Delta\varphi$ for collimated projection (incidentally, it will be seen that Takeda's result does not correspond to that case). The corresponding configuration is in Fig. 16. For collimated projection, the fringes are regularly spaced on any plane because the beam coming from the projector is a parallel beam.

We give here a 2D construction. The 3D construction is deduced from the 2D one owing to $X_B = -G_p x$, $X = -G_c x$.

As previously, the calculation of the phase $\varphi(x, y)$ is performed considering the surface Σ as reflecting surface; afterward, $\varphi_0(x, y)$ is deduced for the surface R ($h = 0$ in this case). The ray BbA' is considered, with

$$\varphi(x, y) = \omega_p Y_B, \quad (\text{B1})$$

where $Y_B = \overline{O_c B}$ on the projector grating.



In the crossed-optical-axes geometry [Fig. 16(a)], we define b_0 as the point of the ray Bb intercepting the plane R and b_1 as the vertical projection of b onto R . It is easy to see that $\overline{Ob_0} \cos\theta = \overline{O_c B}$ and $\overline{b_1 b_0} = h \tan\theta$ (also, $\overline{Ob_1} \equiv y'$). We deduce that $\varphi(x, y) = \omega_p \cos\theta \overline{Ob_0} = \omega_p \cos\theta (y' + h \tan\theta)$, and thus

$$\varphi(x, y) = \omega_p \cos\theta y + \omega_p \sin\theta h (1 - \cot\theta y/L). \quad (\text{B2})$$

It follows that

$$\varphi_0(x, y) = \omega_p \cos\theta y \quad (\text{B3})$$

and the phase difference is

$$\Delta\varphi(x, y) = \omega \sin\theta h (1 - \cot\theta y/L), \quad (\text{B4})$$

where $\omega = \omega_p \cos\theta$ is the frequency of the regularly spaced fringes on R . On a point A' of the camera grating, the intensity is given by the intensity of the point A on the projector grating with $y/L = -Y_A/f_c$. We still have $h = h(x', y')$ with $x' = x - xh/L$ and $y' = y - yh/L$.

Note that our expression of the phase $\varphi(x, y)$ in Eq. (B2) agrees with that of Rajoub (Eq. (9) in [16]) and with [24,25]. In these references, the phase difference $\Delta\varphi$ is not considered. Also, in [24,25], additional hypothesis are considered ($\varphi(x, y) \gg \omega_p y$ and $y/L \ll 1$). Finally, our Eq. (B4) agrees with [26].

In the case of parallel-optical-axes geometry [Fig. 16(b)], the relation between Y_B and y' is $Y_B = D + y' (Y_A = D + y)$; thus, the phases are

$$\varphi_0(x, y) = \omega_p (D + y), \quad \varphi(x, y) = \omega_p (D + y'), \quad (\text{B5})$$

from which we deduce (with $x' = x - xh/L$ and $y' = y - yh/L$)

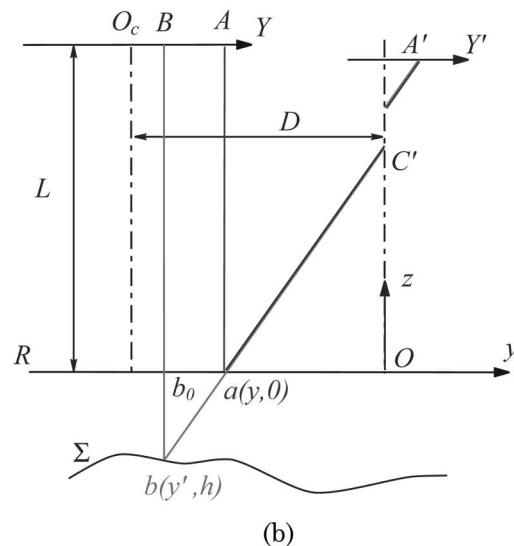


Fig. 16. Collimated projection in the (a) crossed- and (b) parallel-optical-axes geometries.

$$\Delta\varphi(x,y) = -\omega \frac{h(x',y')}{L}y. \quad (\text{B6})$$

Note that the case of parallel-optical-axes geometry cannot be deduced from the calculations in [16].

References and Notes

1. M. Takeda, H. Ina, and S. Kobayashi, "Fourier-transform method of fringe-pattern analysis for computer-based topography and interferometry," *J. Opt. Soc. Am.* **72**, 156–160 (1982).
2. M. Takeda and K. Mutoh, "Fourier transform profilometry for the automatic measurement of 3-D object shapes," *Appl. Opt.* **22**, 3977–3982 (1983).
3. J. Yi and S. Huang, "Modified Fourier transform profilometry for the measurement of 3-D steep shapes," *Opt. Lasers Eng.* **27**, 493–505 (1997).
4. B. Zhao and A. Asundi, "Discussion on spatial resolution and sensitivity of Fourier transform fringe detection," *Opt. Eng.* **39**, 2715–2719 (2000).
5. X. Su, W. Chen, Q. Zhang, and Y. Chao, "Dynamic 3-D shape measurement method based on FTP," *Opt. Lasers Eng.* **36**, 49–64 (2001).
6. Q.-C. Zhang and X.-Y. Su, "An optical measurement of vortex shape at the free surface," *Opt. Laser Technol.* **34**, 107–113 (2002).
7. F. Berryman, P. Pynsent, and J. Cubillo, "A theoretical comparison of three fringe analysis methods for determining the three-dimensional shape of an object in the presence of noise," *Opt. Lasers Eng.* **39**, 35–50 (2003).
8. F. Berryman, P. Pynsent, and J. Cubillo, "The effect of windowing in Fourier transform profilometry applied to noisy images," *Opt. Lasers Eng.* **41**, 815–825 (2004).
9. J. Zhong and J. Weng, "Spatial carrier-fringe pattern analysis by means of wavelet transform," *Appl. Opt.* **43**, 4993–4998 (2004).
10. W. Chen, X. Su, Y. Cao, Q. Zhang, and L. Xiang, "Method for eliminating zero spectrum in Fourier transform profilometry," *Opt. Lasers Eng.* **43**, 1267–1276 (2005).
11. M. A. Gdeisat, D. R. Burton, and M. J. Lalor, "Eliminating the zero spectrum in Fourier transform profilometry using a two-dimensional continuous wavelet transform," *Opt. Commun.* **266**, 482–489 (2006).
12. X. Mao, W. Chen, and X. Su, "Improved Fourier transform profilometry," *Appl. Opt.* **46**, 664–668 (2007).
13. X. Mao, W. Chen, X. Su, G. Xu, and X. Bian, "Fourier transform profilometry based on a projecting-imaging model," *J. Opt. Soc. Am. A* **24**, 3735–3740 (2007).
14. E. Zappa and G. Busca, "Comparison of eight unwrapping algorithms applied to Fourier transform profilometry," *Opt. Lasers Eng.* **46**, 106–116 (2008).
15. X. Su and W. Chen, "Fourier transform profilometry: a review," *Opt. Lasers Eng.* **35**, 263–284 (2001).
16. B. A. Rajoub and M. J. Lalor, "A new phase-to-height model for measuring object shape using collimated projections of structured light," *J. Opt. A Pure Appl. Opt.* **7**, S368–S375 (2005).
17. B. A. Rajoub, M. J. Lalor, D. R. Burton, and S. A. Karout, "A new model for measuring object shape using non-collimated fringe-pattern projections," *J. Opt. A Pure Appl. Opt.* **9**, S66–S75 (2007).
18. Eq. (36) in [17] is rather intricate. For the sake of clarity, it is worth mentioning that our expression for $\varphi(Y)$ gives the same result as their Eq. (36) owing to the correspondences between Rajoub's notations and our notations: $y_{fp} = -D$, $z_{fp} = L_p$, $y_{op} = -D - f_p \sin \theta$, $z_{op} = L_p + f_p \cos \theta$, $z_{fc} = L_c$, $y_{oc} = 0$, $z_{oc} = L_c + f_c$, $Y_i - y_{oc} = Y$, $z_i = h$, and $\omega' = \omega_p / \cos \theta$.
19. The ray bC' has the direction of the vector $(x', y', h - L_c)$ and the ray aC' has the direction of the vector $(x, y, -L_c)$. The cross product of both vectors has to vanish and the first component of the cross product is $xh + (x' - x)L_c$. We get $\delta x \equiv x' - x = -xh/L$.
20. G. S. Spagnolo, G. Guattari, C. Sapia, D. Ambrosini, D. Paoletti, and G. Accardo, "Contouring of artwork surface by fringe projection and FFT analysis," *Opt. Lasers Eng.* **33**, 141–156 (2000).
21. P. Cobelli, A. Maurel, V. Pagneux, and P. Petitjeans, "Fast global measurement of water waves by Fourier transform profilometry," submitted to *Exp. in Fluids*.
22. We have used the unwrapping algorithm *unwrap* from MATLAB (The MathWorks, 2007).
23. The useful relations are $\tan(\theta - \beta) = \overline{Ob'} \cos \theta / L$ and $\tan \beta = (D + y') / (L - h)$, with $y' / (L - h) = y / L$. β is defined in Fig. 13.
24. C. Quan, C. J. Tay, H. M. Shang, and P. J. Bryanston-Cross, "Contour measurement by fibre optic fringe projection and Fourier transform analysis," *Opt. Commun.* **118**, 47983 (1995).
25. F. Lilley, "An optical 3-D body surface measurement system to improve radiotherapy treatment of cancer," Ph.D. thesis, Faculty of General Engineering (Liverpool John Moores University, 1999).
26. L. C. Fang and L. Yang, "A new approach to high precision 3-D measuring system," *Image Vis. Comput.* **17**, 80514 (1999).